Heliyon 10 (2024) e30592

Contents lists available at ScienceDirect

Heliyon

journal homepage: www.cell.com/heliyon

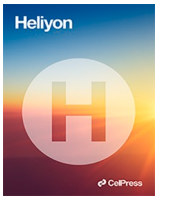

Research article

Unique solvation structure induced by anionic Cl in aqueous zinc ion batteries

Liyuan Jiang, Yulin Zhou, Yan Jiang, Zongyao Zhang, Zhengdao Li, Xinxin Zhao, Jianbao Wu *

School of Mathematics, Physics and Statistics, Shanghai University of Engineering Science, 333 Longteng Road, Shanghai, 201620, China

ARTICLE INFO

Keywords:
AZIBs
Solvation structure
Dissolving effect
Metal cation cluster
ESP

ABSTRACT

Aqueous zinc ion batteries (AZIBs) have garnered significant attention in large-scale static energy storage battery systems due to their low cost, high safety and environmental friendliness. However, it has some inherent problems during operation, such as the occurrence of side reactions (hydrogen evolution reaction, HER) and anode corrosion, formation of by-products and growth of metal dendrites. To analyze the mechanism of generation from aspect of the electrolyte solvation structure and make cell efficiency further improvements based on it, so we use DFT calculations to find the most stable solvation structure in AZIBs with $ZnCl_2$ as the electrolyte and analyze it. We define the relative concentration C_r, and calculate different groups metal cation cluster structures such as $[Zn(H_2O)_n]^{2+}$, $[ZnCl(H_2O)_n]^{+}$, $[ZnCl_2(H_2O)_n]$ and $[ZnCl_3(H_2O)_n]^{-}$ that exist at different C_r. We discuss the effect of different clusters formed due to the C_r variations on the battery performance in terms of three aspects: the structural conformation, the cluster characteristics (including the hydrogen bonding network, bond lengths, bond angles, as well as the electrostatic potential ESP) and the cluster performance (including the adsorption energy E_a, binding energy E_b, and desolvation energy E_{des}). The results shows that the electrolyte metal cation Zn^{2+} can be coordinated with up to six H_2O molecules in first shell, and this metal cation solvation structure contributes to the occurrence and formation of side reactions and by-products, which reduces the battery efficiency. Increasing the electrolyte anion Cl^- concentration by appropriately increasing the C_r helps to desolvate the metal cation cluster structure, which greatly improves the battery efficiency and suppresses the side reactions and by-products. Yet the improvement effect was not obviously further improved by further increasing the Cl^- concentration.

1. Introduction

The trend in batteries is shifting that are more eco-friendly, secure, and sustainable, with an increasing variety of types and better performance [1–7]. Xu [8] was the first to prepare an aqueous zinc ion battery (AZIBs) in 2014, using electrolyte of weakly acidic salt $ZnSO_4$. As a potential candidate for large-scale static energy storage, AZIBs possess several significant advantages: enhanced safety which is eliminating of fire and explosion hazards, reduced cost due to abundant availability of zinc resources and enhanced efficiency (theoretical capacity 820 mA h g^{-1}, redox potential −0.76 V vs. SHE) [9–11]. However, despite the considerable assurance in terms of

* Corresponding author.
E-mail address: wujianbao@sues.edu.cn (J. Wu).

https://doi.org/10.1016/j.heliyon.2024.e30592
Received 23 January 2024; Received in revised form 23 April 2024; Accepted 30 April 2024
Available online 4 May 2024

safety, AZIBs still face multifaceted challenges. During discharging process, Zn is stripped out and solvated to form a structure $[Zn(H_2O)_6]^{2+}$ making its volume larger, thereby unable to effectively enter to the cathode micropores. During the charging process, as the metal cation clusters migrate towards the anode, the desolvation of Zn^{2+} is accompanied by side reaction, the Hydrogen Evolution Reaction (HER) and production of by-products. Simultaneously, spontaneous corrosive reactions at the anode generate H_2. Additionally, uneven anode surface is prone to "tip effect", leading to metal dendrite problems [12,13]. These challenges results in a reduction in the amount of available zinc and seriously affect the efficiency of the batteries. It is imperative to conduct a comprehensive analysis of the solvation structure of electrolyte and effectively address these challenges from an electrolyte perspective. Although the electrolyte does not actively participate in the electrochemical reaction and serves as a supporting component, it plays an essential role within the battery system. The design of the electrolyte plays a pivotal role in ensuring the battery's precise performance at its designated specific capacity. The electrolyte components can regulate the solvation structure and Zn^{2+} desolvation behavior, and change the solvation structure of the electrolyte by adding additives or co-solvents, so as to improve the compatibility between the electrolyte and the electrode and the battery performance and the battery efficiency [14,15].

It can be implemented through three mainstream improvement strategies. Firstly, to establish a eutectic system, Geng [16] developed an innovative eutectic electrolyte comprising ethylene glycol (EG) and $ZnCl_2$ to enable dendrite-free and long-lasting AZIBs. The second is to modify the distribution of hydrogen bonding networks. Previous studies have demonstrated that this can be achieved by incorporating polar additive electrolytes such as N-methyl-2-pyrrolidone (NMP), Tetramethylurea (TMU), Polyaniline (PANI), 2, 2, 2–trifluoroethanol (TFE), and polyhydroxylated organic molecular trehalose [17–21] and modulating the coordination microenvironment using zinc phenolsulfonate and tetrabutylammonium 4-toluenesulfonate as a family of electrolytes [22]. Regulation of the Zn^{2+} solvation structure, promotion of planar zinc deposition, increase in overpotential for hydrolysis reactions, and enhancement of corrosion resistance of zinc anodes in electrolyte also can be facilitated simultaneously. The third is other novel approaches such as preparation of zinc salts, such as a unique zinc salt $Zn(BBI)_2$ with an amphiphilic molecular structure and a safe and non-toxic salt, zinc gluconate, sodium gluconate. These salts can carry out stable and efficient galvanizing/stripping electrochemical reaction and effectively regulates solubility and interfacial conditions [23–25].

According the experiments conducted by Wang [26] demonstrated that $ZnCl_2$ outperformed the other common salts. In this paper, computational experiments have illustrated that in AZIBs utilizing $ZnCl_2$ as the electrolyte, coordination occurs between solvent water molecules and the electrolyte $ZnCl_2$, resulting in the formation of a distinct solvation structure which significantly impacts battery performance. Upon the addition of a zinc chloride molecule to an aqueous solution, the metal cation Zn^{2+} undergoes a solvation phenomenon, wherein it forms bonds with H_2O as ligands. The anionic ligand positions are occupied by water molecules and arranged at the periphery, resulting in the formation of Zn^{2+} solvation structures such as $[ZnCl_2(H_2O)_{100}]$. In this structure, Zn^{2+} is coordinated with six water molecules and undergoes chemical hydration to form $[Zn(H_2O)_6]^{2+}$, which is first shell structure. That the chloride anion plays a pivotal role in the desolvation process of hydrated zinc ion clusters within $ZnCl_2$ electrolyte is elaborated in Ref. [26]. Relevantly, we conducted a comprehensive investigation into the diverse solvation structures present in varying concentrations within the $ZnCl_2$ electrolyte. In order to quantitatively characterize the change in electrolyte concentration during the process, we define the relative concentration C_r as described in Equation (1) of the Supporting Information (SI). By employing this formula, we performed calculations to determine the relative concentrations of all clusters discussed in this article. Subsequently, a table presenting the relative concentration values and a gradient curve illustrating the changes in relative concentration (Fig. S1) were generated. Based on

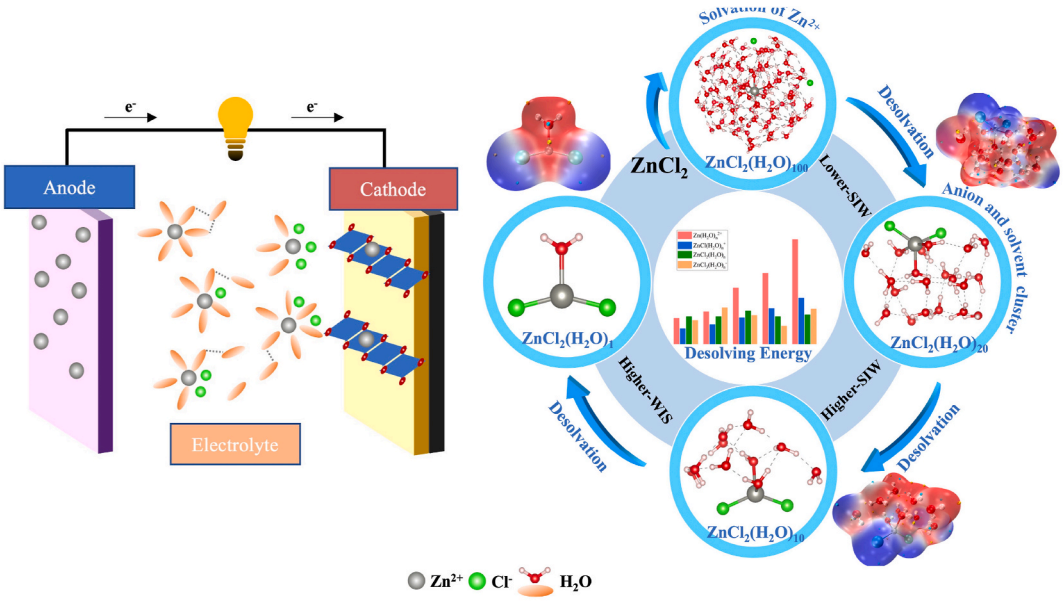

Fig. 1. Left: Distinct solvation structures of $ZnCl_2$; Right: Desolvation process of Cl^- coordination and desolvation energy (E_{des}).

the WIS formula [27] and the relative concentration gradient curves, the electrolyte concentration in this article is further subdivided, we have categorized the relative concentration C_r into four concentration intervals: L-SIW, H–SIW, L-WIS, H-WIS. Referred to as note 1 in the SI, a comprehensive breakdown can be found for further details.

The changes in electrolyte salt concentration were quantitatively characterized by varying the number of bivariate Cl^- ions (y) and water molecules (n), thereby influencing the C_r. In the clusters with different concentration ranges, with the C_r increases, the coordination number of water molecules to Zn^{2+} decreases, allowing Cl^- to rebind with Zn^{2+} and reducing the number of water molecules driven by zinc ion clusters during their movement. Therefore, in AZIBs employing $ZnCl_2$ as the electrolyte, appropriately increasing the electrolyte concentration and the number of chloride ions can significantly enhance battery efficiency and suppress side reactions and by-product formation. However, computational experiments revealed that further elevating the concentration did not yield additional improvements. The solvation structure of electrolyte cationic Zn^{2+} as well as the desolvation process of Zn^{2+} solvation structure clusters through C_r raising and Cl^- assisting, is schematically illustrated in Fig. 1.

2. Computational methods

The cluster structure search and global optimization in this study were initially conducted using a software based on the artificial bee colony algorithm ABCluster [28,29], which has been demonstrated to be highly effective in exploring stable cluster structures in previous article [30,31].

The local optimization and electronic property calculations were performed using the B3LYP [32] hybridization generalization in the Gaussian 16 [33], based on the first principle of density functional theory (DFT). For structure optimization and vibrational frequency calculations, the 6–31g(d) [34–39] basis set was employed. By eliminating imaginary frequencies, it is demonstrated that our derived structure exhibits stability and reasonable efficiency. In the cluster performance part, we use the more accurate base group 6–311+g(d, p) in SMD implicit water solvent model, considering the influence of diffusion function and the overlapping effect of anions, and introduce BSSE correction for calculation.

In this study, we employ the electrostatic potential (ESP) for cluster characterized analysis, which quantitatively describes the charge distribution on the van der Waals surface of clusters. ESP proves effective in predicting and analyzing ion-binding sites and thermodynamic properties. The defining equation of ESP can be found in SI Equation (2) [40–42]. Our analysis utilizes electrostatic potential to investigate ion-binding site characteristics and elucidate the most stable structure as well as unique conformations within a single cluster. Additionally, we examine changes in the overall ESP trend to explain variations in cluster families. The calculated wavefunctions were utilized for the computation of ESP-related data through quantitative molecular surface analysis and electrostatic potential evaluation algorithms using Multiwfn software. Meanwhile, the structural properties were analyzed employing the molecular polarity index (MPI) function, as defined in SI Equation (3) [43–46]. Furthermore, VMD software [47] is employed to generate visual representations of electrostatic potentials.

The Reaction process and calculation methodology for adsorption energy (E_a), binding energy (E_b), and desolvation energy (E_{des}) of all clusters in this study is presented in equations (4)-(7) as detailed in the SI.

3. Result and discussion

In this section, we will investigate the diverse cluster structures that may be formed in $ZnCl_2$ electrolytes at different concentrations and analyze their structural conformation, characteristics, and performance. We will discuss the effect of different clusters formed due to the C_r variations on the battery performance in terms of three aspects: the structural conformation, the cluster characteristics (including the hydrogen bonding network, bond lengths, and bond angles, as well as the electrostatic potential, ESP), and the cluster performance (including the adsorption energy, E_a, binding energy, E_b, and desolvation energy, E_{des}). Aim to meticulously comprehend and analyze the cluster structural conformation at different Cl^- concentrations, employ the control variable method for analysis. We define the general formula $[ZnCl_y(H_2O)_n]^{2-y}$ to represent the electrolyte metal cation and/or anion hydration cluster. We employed a single Zn^{2+} and denoted y as the number of Cl^- and n as the number of hydrations. These variables were grouped based on y (=0, 1, 2, 3) and further arranged in ascending order of n as presented in Table S1. To gain a comprehensive understanding and analysis of how changes in relative concentration gradient impact both metal cation cluster solvation process and desolvation process, it is advisable to holistically analyze them according to the size order of relative concentration gradient as demonstrated in Table S2.

3.1. Analysis of cluster structural conformation

Firstly, we consider the scenario where only Zn^{2+} is introduced into the aqueous solution, $y = 0$. In the pure aqueous solution system, the interaction force between water molecules is solely attributed to hydrogen bonding. Upon the introduction of Zn^{2+} into the system, its presence induces structural alterations. Specifically, it leads to a gradual reduction in strong hydrogen bonding within the original aqueous system while promoting an increase in weak hydrogen bonding. Furthermore, as salt concentration rises, there is a progressive disruption of the net-like structure formed by hydrogen bonds. Due to the unique properties of zinc ions, such as their small ionic radius, multivalent (2-valent) charge, high electronegativity, and strong electric field, the original hydrogen-bonding structure of pure aqueous solution is disrupted. Consequently, water molecules no longer predominantly form hydrogen bonds with each other but instead preferentially bind with Zn^{2+}. As a result, the solution undergoes reconstitution, forming a solvated structural system wherein the primary structure consisted of the first shell of Zn^{2+}. As the value of n increases from 1, Zn^{2+} undergoes hydration with water molecules and initiates the formation of its first solvated shell, denoted as $[Zn(H_2O)_n]^{2+}$. This structural arrangement arises due to the

coordination between the one lone electrons pair provided by the O in each H_2O molecule and the vacant orbitals of Zn^{2+}, resulting in chemical hydration and bond formation to establish primary water of hydration. The primary hydrated water is tightly bound to Zn^{2+}, restricting their mobility and accompanying the ions. When $n \in [1,6]$, water molecules continue to bind to the Zn^{2+}, and the number of water molecules in the first shell reaches a plateau at $n = 6$. The hexa-ligand arrangement of water molecules around Zn^{2+} forms an octahedral structure, representing the predominant solvation conformation of Zn ions in AZIBs. With $n > 6$, the first shell remains unchanged while the formation of the second shell initiates, accompanied by hydrogen bonding between molecules in the first and second shell. The emergence of the second shell can be attributed to electrostatic interactions, specifically ion-dipole interactions, as water molecules combine with Zn^{2+}. Water molecules combined at the base of the first shell are called secondary water of hydration, exhibits weak binding forces due to their considerable distance from the central ions and often remain immobile relative to the ions. The hydrogen bonding network between water molecules gradually strengthens as the number of water molecules increases, resulting in the presence of not only hydrogen bonding between first shell and second shell but also intermolecular hydrogen bonding within the same layer, as shown in Table 1(a). It has been observed that the hydration number n in first shell of $[Zn(H_2O)_n]^{2+}$ has been demonstrated a maximum value of $n_{Max} = 6$ [48,49]. The H_2O molecule is known to possess two H atoms, capable of forming hydrogen bonds with two water molecules, as well as two lone electron pairs on the O atoms, facilitating the formation of two hydrogen bonds with other H atoms in H_2O. Consequently, a single H_2O molecule can engage in up to four hydrogen bonds. In the first shell, each of the six O atoms contributes a lone electrons pair and combines with Zn^{2+} empty orbitals through coordination bonding. As a result, each water molecule can potentially form hydrogen bonds with up to three water molecules in the second shell. In essence, this implies that the maximum number of water molecules within the second shell could reach 18.

For $y = 1$, the water molecules exhibit a similar bonding pattern to that of $[Zn(H_2O)_n]^{2+}$. however, there is a significant disparity in the bonding location. In contrast to the uniform octahedral bonding configuration observed in the first shell of $[Zn(H_2O)_n]^{2+}$, the water molecules in $[ZnCl(H_2O)_n]^{+}$ exhibit a convergent bonding position on the opposite side of Cl^-. Fig. 2(a) reveals that a water molecule exhibits a negative charge field surrounding the O and a positive charge field distributed around the H. Through electrostatic interaction, as depicted in Fig. 2(b), $[ZnCl]^+$ form ionic bonds between Cl^- and Zn^{2+}. Subsequently, guided by the principles of charge homogeneity repulsion and anisotropy attraction, Fig. 2(c) demonstrates that the bonding position of the water molecule with Zn^{2+} is predominantly located on the opposite side of Cl^- in $[ZnCl(H_2O)]^+$. The addition of Cl^-, when $y = 1$ and $n = 4$, a single H_2O does not provide sufficient energy for altering the bonding positions of the other three H_2O molecules, thereby it is arranged in the second shell through hydrogen bonding formation instead of binding in first shell. Consequently, compared to $[Zn(H_2O)_n]^{2+}$, the time required for hydrogen bonding formation in this cluster family is advanced, while reaching saturation in the first shell is delayed until $n = 10$, as depicted in Table 1(b).

For $y = 2$, this cluster family is electrically neutral. The bonding positions of the ions exhibit both similarities and differences when

Table 1
Cluster structure of $[Zn(H_2O)_n]^{2+}$, $[ZnCl(H_2O)_n]^{+}$, $[ZnCl_2(H_2O)_n]$ and $[ZnCl_3(H_2O)_n]^{-}$.

(a) $[Zn(H_2O)_n]^{2+}$	1	2	3	4	5	6	7	8	9
	10	15	16	17	18	19	20	25	30
(b) $[ZnCl(H_2O)_n]^{+}$	0	1	3	4	6	7	9	10	15
(c) $[ZnCl_2(H_2O)_n]$	0	1	2	3	4	6	10	15	20
(d) $[ZnCl_3(H_2O)_n]^{-}$	0	1	2	3	4	5	8	10	15

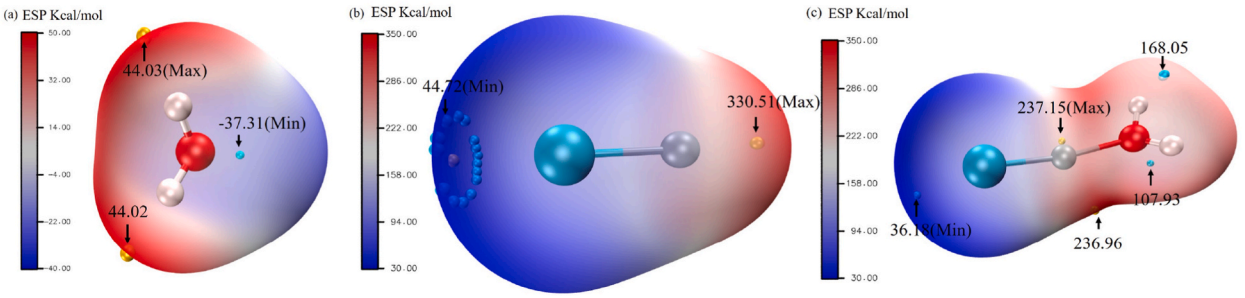

Fig. 2. Electrostatic potential diagram (a)H_2O; (b) $[ZnCl]^+$; (c) $[ZnCl(H_2O)]^+$; Yellow ball: the point where the value of electrostatic potential is maximum; Blue ball: the point where the value of electrostatic potential is minimum. (For interpretation of the references to colour in this figure legend, the reader is referred to the Web version of this article.)

compared to those aforementioned cluster families. Specifically, this family of cluster contains two Cl^- which exhibit a slightly more intricate structure formation and ionic bonding positions compared to the $[ZnCl(H_2O)_n]^+$ and $[Zn(H_2O)_n]^{2+}$ cluster families. When n = 1, the Cl^- ions are symmetrically distributed on both sides of Zn^{2+}, while the O interact with Zn^{2+} through coordination bonding. As the n increases, the individual water molecules become hardly to disrupting the formed structure of the higher energy cluster. Consequently, these water molecules align themselves to formed new cluster in hydrogen-bonded manner. Until n = 4, the energy associated with hydrogen bonding network formed by water molecules manages to disrupt the formed cluster structure and coordination to form new Zn–O bond. This observation suggests again that an increase in y and elevated salt concentration leads to an earlier formation time for hydrogen bonds and delays the saturation time required for reaching the first shell, as depicted in Table 1(c).

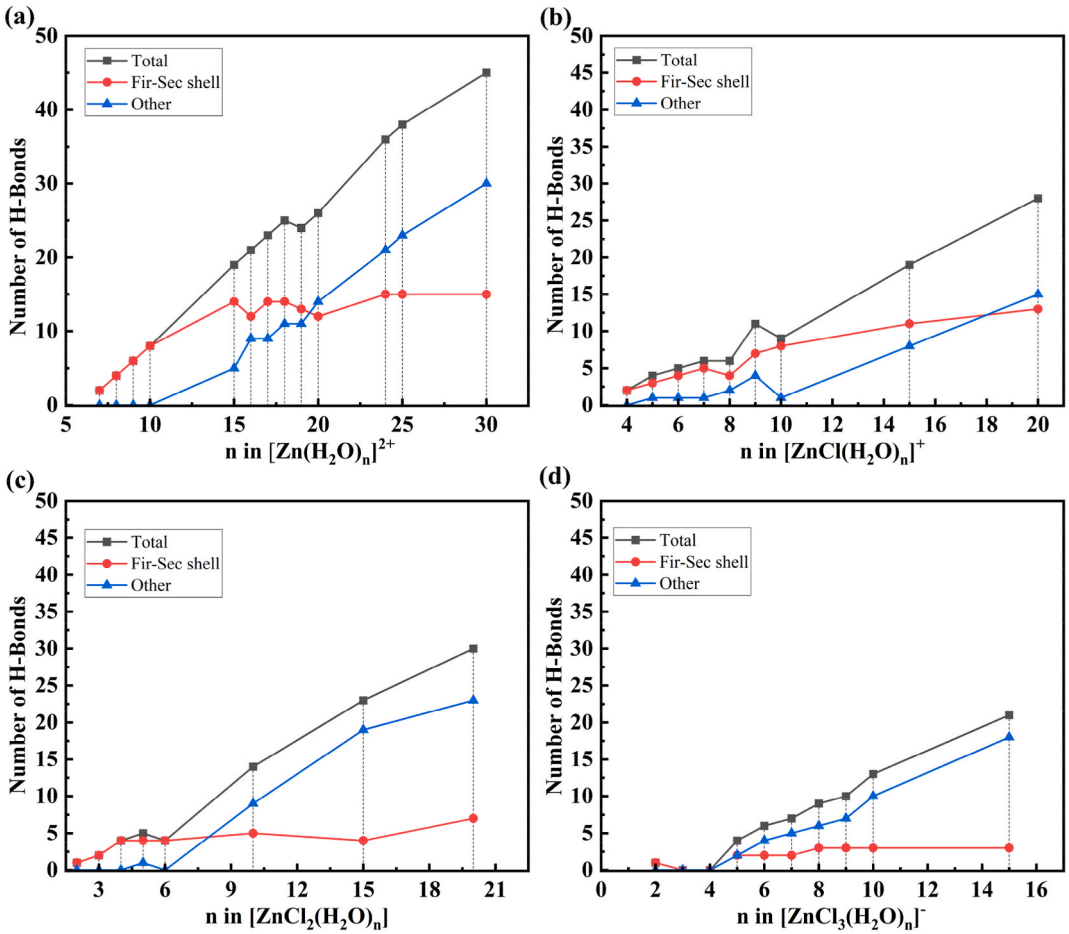

Fig. 3. Hydrogen bonds numbers of $[ZnCl_y(H_2O)_n]^{2-y}$ (Fir-Sec shell: the Hydrogen bonds numbers of between molecules in the first and second shell.). (a) $[Zn(H_2O)_n]^{2+}$; (b) $[ZnCl(H_2O)_n]^+$; (c) $[ZnCl_2(H_2O)_n]$; (d) $[ZnCl_3(H_2O)_n]^-$.

For y = 3, the Cl^- concentration continues to increase, leading to clusters exhibit an overall negative charge. The structural conformation of this cluster family exhibits significant disparities compared to aforementioned clusters, owing to the transition in electrical properties from positive to negative. As the y increases further, it becomes increasingly challenging for water molecules to bind to the cluster and they tend to align themselves in a hydrogen-bonding arrangement, impeding the attainment of a saturated state by the first shell. When n = 1, the Zn^{2+} is encapsulated by three Cl^- ions, forming a monolithic structure with a negative electric field. Consequently, the water molecule is unable to approach the central Zn^{2+} in this scenario, which can only align themselves with H facing the Cl. Thus, under these conditions, the Zn^{2+}, Cl^-, H_2O molecules are arranged coplanarly. When n = 3, a network of hydrogen bonds is established among the three water molecules, aligning them closely in a nearly coplanar arrangement that is almost perpendicular to the plane occupied by the Cl–Zn. Similarly, this arrangement persists when n = 4. However, for n = 5, the energy of hydrogen bonding network among water molecules can be enough to disrupt the formed cluster and coordination a Zn–O bond, as depicted in Table 1(d).

3.2. Analysis of cluster characteristics

In this section, we will discuss the pertinent characteristics of cluster families $[Zn(H_2O)_n]^{2+}$, $[ZnCl(H_2O)_n]^+$, $[ZnCl_2(H_2O)_n]$ and $[ZnCl_3(H_2O)_n]^-$ in terms of their hydrogen bonding network, bond lengths and angles, as well as electrostatic potentials. The corresponding common parameters for these cluster families are presented in Tables S3, S4, S5 and S6.

3.2.1. Hydrogen bonding network

Comparison of groups: The analysis reveals both similarities and differences in the hydrogen bonding networks among the four cluster families. Similarly, as n increases, all four cluster families exhibit trend of increase in the number of hydrogen bonds between first shell and second shell and other hydrogen bonds. When number of water molecule reaches a certain scale, the hydrogen bonds between first shell and second shell essentially reach a state of saturation, while the number of other hydrogen bonds gradually surpasses the number of hydrogen bonds between first shell and second shell. The difference lies in the fact that at y = 0, as the hydration number of $[Zn(H_2O)_n]^{2+}$ increases, particularly after reaching saturation in the first shell ($n \geq 7$), the solvation effect of Zn^{2+} is enhanced. This results in an increase in hydrogen bonding, larger cluster volumes, and a decrease in movement rate, ultimately leading to a reduction in battery coulomb efficiency. However, when y = 1, the energy of these newly added water molecules cannot easily alter the structure of the formed clusters. Therefore, they tend to arrange and combine into new clusters through hydrogen bonding, resulting in an acceleration of hydrogen bonding formation time for Zn^{2+} solvation clusters and a delay in the saturation time of the first shell, as shown in Fig. 3. The saturation of $[Zn(H_2O)_6]^{2+}$ is achieved, whereas $[Zn(H_2O)_7]^{2+}$ gradually forms intermolecular hydrogen bonding. When the first shell of $[ZnCl(H_2O)_4]^+$ is not saturated, two hydrogen bonds has been formed, and the saturation time of the first shell is delayed until $[ZnCl(H_2O)_{10}]^+$ reaches its saturation state. When y = 2, the hydrogen bonding of $[ZnCl_2(H_2O)_2]$ has been appeared, however, the saturation time of the first shell is further delayed, $[ZnCl_2(H_2O)_{20}]$ remains unsaturated. Furthermore, when y = 3, the water molecules can only tightly enclose the cluster making it challenging to arrange hydrogen bonds and even predict the time required to reach first shell saturation. The saturation time of the hydrogen bond between first shell and second shell also advances with increasing y. The number of other hydrogen bonds surpasses the number of hydrogen bonds between first shell and second shell after $n \geq 18$ in $[Zn(H_2O)_n]^{2+}$, however it has been surpassed that $n \geq 5$ in $[ZnCl_3(H_2O)_n]^-$. Simultaneously, the number of hydrogen bonds between first shell and second shell that reach saturation decreases from more than 10 at y = 1 to 3 at y = 3. The solvation structure of Zn^{2+} gradually disintegrated as y increased. The coordination number of water molecules in the first shell decreased progressively from highest 6 in $[Zn(H_2O)_6]^{2+}$ to lowest 1 in the $[ZnCl_3(H_2O)_{20}]^-$, indicating that the addition of Cl^- facilitated the desolvation process of Zn^{2+}. Therefore, an increase in the concentration of Cl^- accelerates the formation of cluster hydrogen bonds and delays the saturation time of the first shell. Additionally, it advances the saturation time and reduces the amount of hydrogen bonding between first shell and second shell, indicating that a certain quantity of chloride ions facilitates desolvation of solvated metal cations.

Comparison of electrolyte relative concentration as a whole: Comparison of the C_r of different cluster families upon reaching saturation of first shell layer. $C_{r_{[Zn(H_2O)_6]^{2+}}}^{y=0} = 0.60$ at H–SIW, $C_{r_{[ZnCl(H_2O)_{10}]^+}}^{y=1} = 0.56$ at H–SIW, $C_{r_{[ZnCl_2(H_2O)_n],n\geq 20}}^{y=2} < 0.380$ at L-SIW. It can be observed that as the concentration of Cl^- y increases, the n of clusters required to reach the saturated state of the first shell also increases and this is found that their C_r is decreased gradually, indicating that a decrease in salt concentration makes it easier for clusters to reach saturation in the first shell, the state of C_r required to reach this state is between L-SIW and H–SIW. Conversely, an increase in salt concentration makes this process more difficult, when the state of C_r between L-WIS and H-WIS. Similarly, by comparing the concentrations of different clusters during the initial formation of the hydrogen bond between first shell and second shell, $C_{r_{[Zn(H_2O)_7]^{2+}}}^{y=0} = 0.51$ at H–SIW; $C_{r_{[ZnCl(H_2O)_4]^+}}^{y=1} = 1.40$ at L-WIS, $C_{r_{[ZnCl_2(H_2O)_2]}}^{y=2} = 3.79$ at H-WIS, $C_{r_{[ZnCl_3(H_2O)_2]^-}}^{y=3} = 4.78$ at H-WIS. The decrease in the required n for cluster formation of the initial first shell and second shell hydrogen bond can be observed as y increases, accompanied by a gradual increase in their Cr. This suggests that an increase in electrolyte salt concentration and it is between L-WIS and H-WIS, facilitates the formation of the interhydrogen bond between first shell and second shell. Conversely, when in between the L-SIW and the H–SIW cannot be formed. Consequently, the hydrogen bond between first shell and second shell clusters is formed earlier and more easily as the amount of Cl^- increases, the easier it is to form between L-WIS and H-WIS. while it becomes increasingly difficult to reach the saturation state of the first shell with higher electrolyte salt concentrations, it is easier to reach that state between L-SIW and H–SIW.

3.2.2. Bond length and bond angle

Form the whole perspective, The Zn–O bond length $r_{Zn\text{-}O}$ exhibits an increasing trend in $[Zn(H_2O)_n]^{2+}$, $[ZnCl(H_2O)_n]^{+}$ and $[ZnCl_2(H_2O)_n]$, decreasing in $[ZnCl_3(H_2O)_n]^{-}$. The Zn–Cl bond length $r_{Zn\text{-}Cl}$ exhibits an increasing trend in clusters $[ZnCl(H_2O)_n]^{+}$, $[ZnCl_2(H_2O)_n]$ and $[ZnCl_3(H_2O)_n]^{-}$. Due to the larger atomic radius of O compared to Cl, $r_{Zn\text{-}Cl}$ consistently surpasses $r_{Zn\text{-}O}$ across all clusters. The correlation between $r_{Zn\text{-}O}$ and $r_{Zn\text{-}Cl}$ exhibited a positive trend in clusters $[Zn(H_2O)_n]^{2+}$, $[ZnCl(H_2O)_n]^{+}$ and $[ZnCl_2(H_2O)_n]$, while it displayed a negative trend in cluster $[ZnCl_3(H_2O)_n]^{-}$, as depicted in Fig. 4. The greater the bond length, the lower the bond energy., indicating a reduction in interatomic interaction forces. Specially, the formation of the first shell in $[Zn(H_2O)_n]^{2+}$ with hydration number $n \leq 6$ is accompanied by a gradual increase in $r_{Zn\text{-}O}$, indicating a progressive weakening of the Zn and O interaction force with increasing hydration number n. For $n \geq 6$, $r_{Zn\text{-}O}$ fluctuate within the range of 2.09–2.14 Å, with an average convergence at 2.1 Å. These calculations are consistent with published article [26]. It means that the insignificance of the second shell on Zn–O bonding in the first shell is indicated, thereby confirming that the hydrogen bonding force between water molecules is smaller than the bonding force between Zn–O. Similarly, $[ZnCl(H_2O)_n]^{+}$ and $[ZnCl_2(H_2O)_n]$ exhibit a continuous growth trend of $r_{Zn\text{-}O}$ and $r_{Zn\text{-}Cl}$ with weakened interatomic interactions prior to reaching saturation in the first shell. However, once the first shell is saturated, both $r_{Zn\text{-}O}$ and $r_{Zn\text{-}Cl}$ remain essentially unchanged. For instance, stabilization of bond lengths after $[ZnCl(H_2O)_{10}]^{+}$. $[ZnCl_2(H_2O)_{20}]$ has not yet been saturated, thus the $r_{Zn\text{-}O}$ and $r_{Zn\text{-}Cl}$ continue to growth. In contrast to the other three cluster families, it is increasing difficultly for water molecules to establish bonds in $[ZnCl_3(H_2O)_n]^{-}$ due to the maximum concentration of Cl^{-}. Consequently, the chloride ions create a competitive relationship with the oxygen atoms, forming ligand-competitive interactions. When $n \geq 5$, the energy of the hydrogen bond network of H_2O cluster counteracts the $[ZnCl_3]^{-}$, leading to the formation of a Zn–O bond with a decreasing $r_{Zn\text{-}O}$, indicating an enhanced interaction force between Zn^{2+} and O. Conversely, $r_{Zn\text{-}Cl}$ continues to increase, suggesting a weakening of the interaction force between Zn^{2+} and Cl^{-}. As the hydrogen bonding network reaches a certain scale, such as when n is greater than or equal to 10, an equilibrium state is achieved between $r_{Zn\text{-}O}$ and $r_{Zn\text{-}Cl}$, which remains essentially unchanged.

With the gradual increase of n, the average bond angle $\Theta^{ave}_{O\text{-}H\text{-}O}$ of water molecules in the first shell of the four cluster families exhibits minor fluctuations within a narrow range between 100° and 110°, as depicted in Fig. 5. This phenomenon can be attributed to the binding arrangement of water molecules with zinc ions exhibits an increasingly homogeneous and symmetrical distribution as n increases, resulting in minimal mutual influence among water molecules and consequently larger bond angles ∠O–H–O. As the n continues to increase, the spacing between water molecules decreases, leading to a gradual increase in their mutual influence and

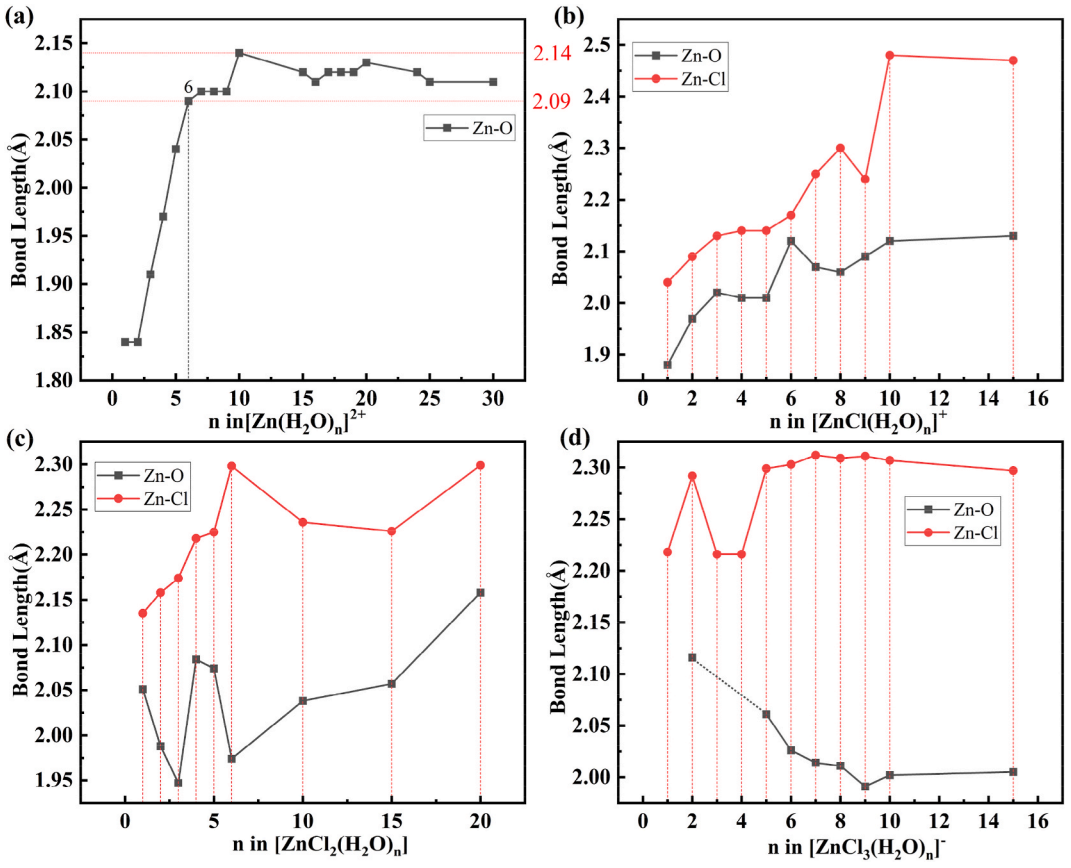

Fig. 4. Bond length of $[ZnCl_y(H_2O)_n]^{2-y}$; (a) $[Zn(H_2O)_n]^{2+}$; (b) $[ZnCl(H_2O)_n]^{+}$; (c) $[ZnCl_2(H_2O)_n]$; (d) $[ZnCl_3(H_2O)_n]^{-}$.

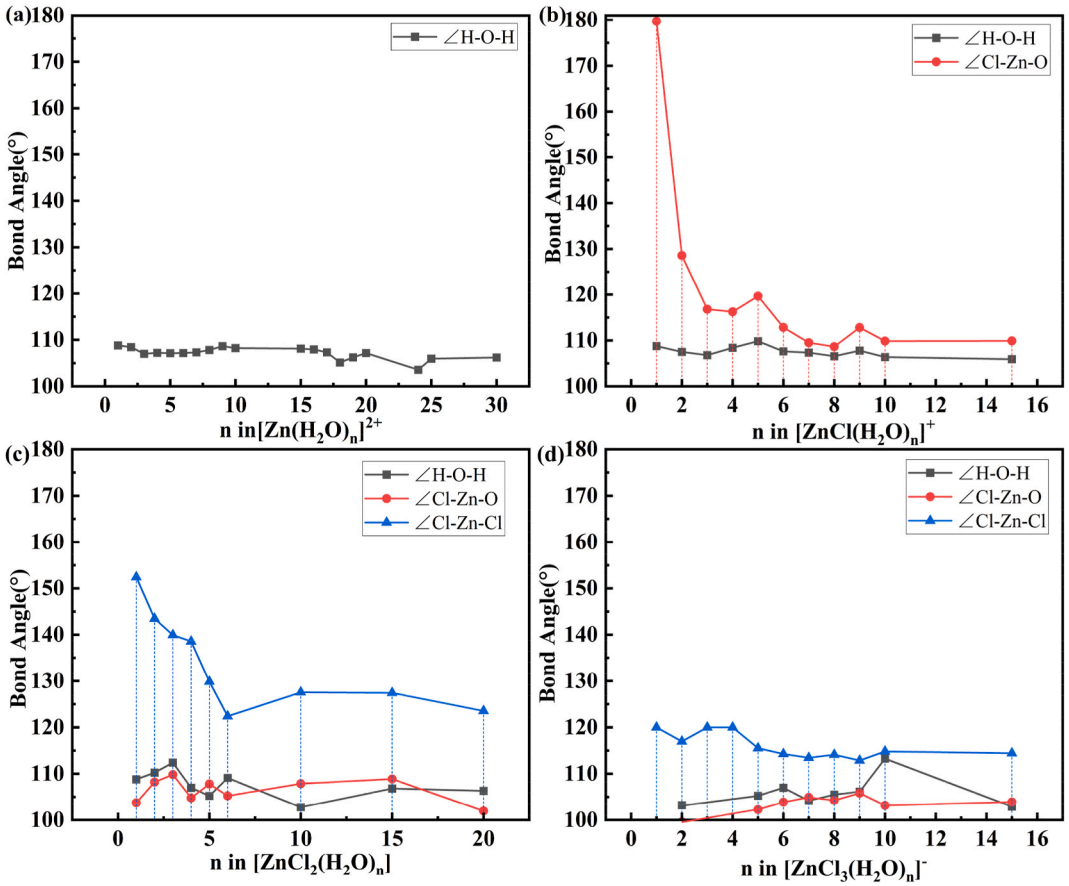

Fig. 5. Bond angle $\Theta^{ave} = \frac{\theta_1+\cdots+\theta_n}{n}$ in the first shell of $[ZnCl_y(H_2O)_n]^{2-y}$; (a) $[Zn(H_2O)_n]^{2+}$; (b) $[ZnCl(H_2O)_n]^{+}$; (c) $[ZnCl_2(H_2O)_n]$; (d) $[ZnCl_3(H_2O)_n]^{-}$.

strengthening of interaction. Simultaneously, the repulsive force also intensifies due to the strengthening hydrogen bonding network, resulting in more closely arranged of water molecules and a slight fluctuation trend observed in $\Theta^{ave}_{O\text{-}H\text{-}O}$.

The average bond angle $\Theta^{ave}_{Cl\text{-}Zn\text{-}O}$ of ∠Cl–Zn–O in the first shell exhibits a sharp decrease followed by stabilization in $[ZnCl(H_2O)_n]^{+}$., while it demonstrates slight fluctuations within the range of 100°–110° in $[ZnCl_2(H_2O)_n]$ and $[ZnCl_3(H_2O)_n]^{-}$. The ∠Cl–Zn–O in Fig. 5 (b) exhibits a decreasing trend with an increasing of n. When $n \leq 10$, the first shell structure is being formed, and at this stage, water molecules tend to be predominantly distributed on the opposite side of Cl^{-}. This is particularly evident with the addition of the first water molecule, resulting in a larger angle for the ∠Cl–Zn–O, approaching 180°. As more water molecules are added, this angle gradually decreases due to an increasing number of Zn–O bonds. Once saturation is reached in the first shell, however, the angle of the ∠Cl–Zn–O remains relatively unchanged.

The average bond angles $\Theta^{ave}_{Cl\text{-}Zn\text{-}Cl}$ of ∠Cl–Zn–Cl in the first shell exhibit a decreasing trend, all of which are larger than $\Theta^{ave}_{Cl\text{-}Zn\text{-}O}$ and $\Theta^{ave}_{O\text{-}H\text{-}O}$ as depicted in Fig. 5. The ∠Cl–Zn–Cl bond angles demonstrate an overall declining trend due to the increasing number of water molecules, resulting in a gradual increasing number of Zn–O bonds and reaching the status of saturation within the first shell. Consequently, this leads to a more compact arrangement of atoms and reduced atomic spacing within the first shell. Additionally, the strengthening energy of the hydrogen bond network contributes to decrease in ∠Cl–Zn–Cl bond angle. The charge distribution trend of $[ZnCl_2(H_2O)_n]$ (n = 0, 1, 2, 3, 6, 20) is illustrated in Fig. S6. The original ∠Cl–Zn–Cl bond angle in the zinc chloride molecule is 180°. Upon examining Fig. 1(a)–a negative electric field can be observed around the O in water molecule while a positive electric field surrounds H. According to Fig. S4, the electrostatic potential around Zn^{2+}, the central atom of the zinc chloride molecule, exhibits a positive electric field and remains neutral between Cl^{-} and Zn^{2+}, whereas a negative electric field is present around Cl^{-}. Consequently, when zinc chloride molecules aggregate with water molecules, ligand bonding occurs between O and Zn^{2+}. Due to oxygen's higher electronegativity compared to chlorine and its stronger electron-attracting ability, this results in a decrease of the ∠Cl–Zn–Cl bond angle from 180° to 152.42° as depicted in Fig. 5(c). This also elucidates the phenomenon of distinct molecular clusters adopting diverse arrangements, wherein water molecules and two chloride ions are positioned on either side of the zinc ions. From the perspective of charge transfer, the charge distribution of the clusters exhibited uniform variation. With each addition of water molecules, there was an observed increase in positive charges for cations within the clusters, such as Zn^{2+} and H^{+}. Specifically, the charge on Zn^{2+} increased from 0.62C (n = 1) to 0.71C (n = 20). Conversely, anions like O^{2-} and Cl^{-} displayed a tendency towards decreasing negative charges, such as the left Cl^{-} charge decreasing from −0.31C (n = 1) to −0.59C (n = 20). This accounts for the increasing strength of the positive

electric field surrounding the water molecules located on the side of the Zn^{2+}, as well as the intensifying negative electric field around the Cl^- on the opposite side, and the charge disparity between the two poles is progressively amplifying. However, this counterpart relationship, strong and weak, contrast is evidently unbalanced. As n continues to increase, leading to a strengthening hydrogen bonding network among them, the transfer of charge in chloride ions is limited. Consequently, when clusters reach a certain number of hydrations, their hydrogen bonding network energy surpasses that energy of chloride ions. The network of water molecules will gradually surround the entire Zn–Cl cluster.

3.2.3. Electrostatic potential

The electrostatic potential (ESP) is responsive to the imbalanced distribution of charge, while polarity similarly characterizes the non-uniformity of the charge distribution. The more uneven the charge distribution, the greater the absolute value of the maximum and/or minimum electrostatic potential values, thereby enhancing polarity strength. The MPI function provides a quantitative description of cluster polarity, whereby larger MPI values indicate a stronger polarity and conversely smaller values suggest weaker polarity. Form the whole perspective, the values of the $|ESP_{max}|$ for the four cluster families exhibit a decreasing trend and eventually stabilize. Similarly, the values of the $|ESP_{min}|$ also demonstrate a gradual decrease and stabilization. The MPI values also shows the same trend as shown in Fig. 6. The gradual from decrease to stabilization of $|ESP_{max}|$ and $|ESP_{min}|$ indicate that the cluster charge distribution undergoes a developmental process from an initial imbalance to gradually achieving balance, ultimately reaching stabilization as the hydration number n increases. Additionally, the polarity gradually diminishes from stronger to weaker due to the enhanced contribution of lone-pair electrons provided by oxygen atoms in water molecules and the occurrence of nucleophilic reactions, resulting in a more uniform charge distribution on the surface of clusters. By dividing each cluster into 20 equal intervals based on the electrostatic potential values ranging from minimum to maximum, we calculated the surface area sum of each interval, as shown in Figs. S2–S5. Our results indicate that as the hydration number n increases, the charge distribution gradually becomes balanced from initial imbalance and the surface area in the averaged state also increases. The trend of surface area change confirms a development of cluster charge distribution from unbalanced to gradually balanced and finally to stabilization with increasing hydration number n, while polarity decreases.

By comparing the changes of ESP before and after water addition, it was observed that the influence of water on the ESP of its molecules gradually diminished with increasing y. This implies that as the concentration of chloride ions increased, their effect on the ESP of clusters became increasingly dominant. With an increasing Cl^- concentration, there was a consistent decrease in ESP_{max}, ESP_{min}, and MPI values of the clusters, accompanied by a shift from $+2$ valence to -1 valence charge distribution. As y increased from 0 to 2, there was a general reduction in MPI value indicating a gradual decrease in cluster polarity and more uniform charge distribution. However, when the value of y reached 3, there was an unexpected increase in MPI due to a transition from neutral to negatively charged clusters and non-uniform charge distribution leading to an increment in polarity.

3.3. Analysis of cluster performance

In this section, we have computed the adsorption energy E_a, binding energy E_b, and successive desolvation energy E_{des} of the clusters to gain a more comprehensive understanding of the properties of the solvated Zn^{2+} clusters and Cl^- ligand at varying electrolyte concentrations C_r. The outcomes of these calculations are illustrated in Fig. 7.

The fact can be ascertained that the E_a of the clusters exhibits a more negative trend and decreases linearly with an increase in hydration number n, indicating that the energy released from the clusters gradually increases as the Cl^- number y increases, $\Delta E_a = E_a^{[ZnCl_y(H_2O)]^{2-y}} - E_a^{[ZnCl_{y+1}(H_2O)]^{1-y}}$ ($kcal \cdot 10^2$ /mol), ΔE_{a1} (0.87, y = 0) > ΔE_{a2} (0.76, y = 2) > ΔE_{a3} (0.75, y = 1). Consequently, an increase in Cl^- concentration leads to a decrease in the cluster adsorption energy, enhancing its stability, however, it simultaneously reduces the charge of the cluster. As n increases, there is an orderly rise in the energy of clusters depicted in Fig. 7(a), indicating their increasing stability.

Similarly, E_b of the clusters decreases with increasing Cl^- concentration, and the rate at which E_b becomes smaller slows down as n increases. This observation indicates that an increase in the number of Cl^- ions leads to more negative for E_b and greater energy

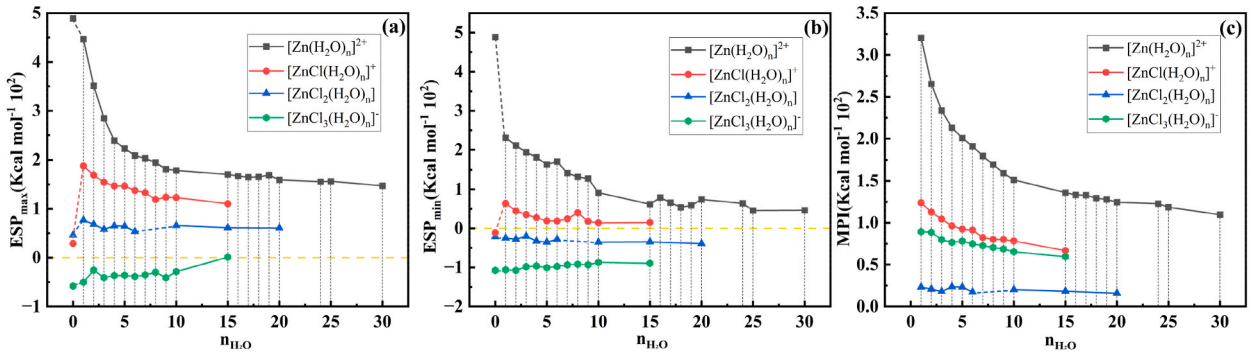

Fig. 6. Electrostatic potential (ESP) and MPI function; (a) The trend of ESP_{max}, (b) The trend of ESP_{min}, (c) The trend of the MPI.

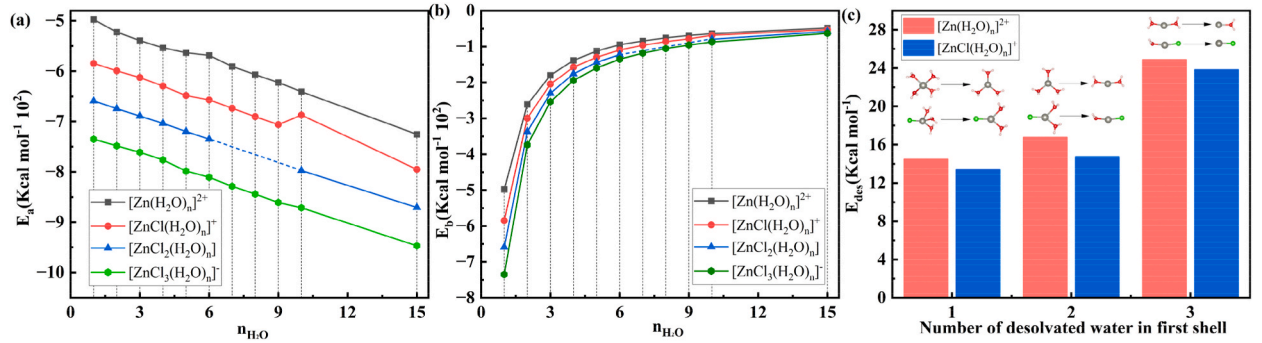

Fig. 7. (a) adsorption energy E_a, (b) binding energy E_b, (c) successive desolvation energy.

release. Moreover, higher concentrations of Cl^- facilitate easier stabilization of the clusters, $\Delta E_b = E_b^{[ZnCl_y(H_2O)_2]^-} - E_b^{[ZnCl_y(H_2O)]^-}$ (kcal·10^2 /mol), ΔE_{b1} (3.61, y = 3) > ΔE_{b2} (3.22, y = 2) > ΔE_{b3} (2.85, y = 1) > ΔE_{b4} (2.36, y = 0). The higher concentration of Cl^- facilitates the stabilization of clusters, as n increases, the clusters gradually stabilize and approach a saturation state, with diminishing differences in E_b of two adjacent clusters between four clusters approaching zero, as depicted in Fig. 7(b).

Next, we will discuss the successive desolvation energy E_{des}, of the cluster. To exclude the effects of hydrogen bond and account for the fact that the first shell, which experiences only chemical hydration, moves with the metal cations during cell operation, we will focus solely on considering dehydration of this first shell. The conclusion can be drawn that the E_{des} increase in a sequential manner from $E_{des}^{[Zn(H_2O)_4]^{2+}} = 14.48$ kcal/mol to $E_{des}^{[Zn(H_2O)]^{2+}} = 24.88$ kcal/mol in the presence of only $[Zn(H_2O)_n]^{2+}$ prior to the addition of Cl^-. This result implies a gradual elevation in the E_{des} with each water molecule removed, which poses a detrimental impact on cell efficiency. After the addition of a single Cl^-, it is evident that the E_{des} experiences a substantial decrease from $E_{des}^{[ZnCl(H_2O)_4]^+} = 13.38$ kcal/mol to $E_{des}^{[ZnCl(H_2O)]^+} = 23.82$ kcal/mol consecutively. Furthermore, there is 4.2 %, 1.05 kcal/mol reduction in the E_{des} for removing the final water molecule. This result elucidates the observation that an increase in electrolyte salt concentration leads to the coordination of Cl^- with Zn^{2+} to form the first shell, thereby reducing the energy for cluster desolvation and enhancing cell efficiency. This phenomenon is indicated that electrolyte concentration effectively facilitates desolvation of solventized metal ion clusters up when it is increasing to a certain concentration.

4. Conduction

The root causes of inherent side reactions and by-products occurrence were analyzed from the perspective of electrolyte solvation structure in aqueous zinc ion batteries to investigate the underlying causes, wherein solvated zinc ion clusters undergo side reactions and by-product as they migrate towards the electrodes during operation, thereby diminishing the efficiency of the cell. With the gradual addition of Cl^-, the coordination reaction between Cl^- and clusters occurs, displacing the original water molecules, indicating a gradual reduction in polarity and the energy of the clusters increases in a systematic manner, while the desolvation energy experiences a significant reduction and the stability of the clusters progressively enhances. However, as the concentration of Cl^- increases, its impact gradually diminishes and eventually becomes negligible. The overall observation reveals that an increase in electrolyte salt concentration facilitates the formation of hydrogen bonds within clusters, while simultaneously hindering their attainment of a saturated state in the first shell. Therefore, in aqueous zinc ion batteries employing $ZnCl_2$ as the electrolyte, appropriately increasing the concentration of Cl^- in the electrode solution will significantly enhance battery efficiency by suppressing side reactions and minimizing by-product formation. However, further increments in its concentration do not yield any substantial additional improvement. In summary, the work presented in this article offers some theoretical underpinnings for comprehending both the electrolyte and the interaction mechanism between the electrolyte and electrode materials. The findings of this study would hold implications for guiding further enhancements in aqueous zinc-ion battery performance.

CRediT authorship contribution statement

Liyuan Jiang: Writing – original draft, Data curation. **Yulin Zhou:** Formal analysis. **Yan Jiang:** Software. **Zongyao Zhang:** Data curation. **Zhengdao Li:** Resources. **Xinxin Zhao:** Formal analysis. **Jianbao Wu:** Writing – review & editing, Project administration.

Declaration of competing interest

There are no conflicts to declare.

Acknowledgements

JBW was supported by the National Natural Science Foundation of China (No. 11047164), the National Key Laboratory of Infrared Detection Technologies (No. IRDT-23-S01), the Shanghai College Foundation for Excellent Young Teachers of China (No. gjd10023) and the Academic Program of Shanghai Municipal Education Commission (No.11XK11 and 2011X34).

Appendix A. Supplementary data

Supplementary data to this article can be found online at https://doi.org/10.1016/j.heliyon.2024.e30592.

References

[1] S. Chu, A. Majumdar, Opportunities and challenges for a sustainable energy future, Nature 488 (7411) (2012) 294–303.
[2] Y. Liang, Y. Jing, S. Gheytani, et al., Universal quinone electrodes for long cycle life aqueous rechargeable batteries, Nat. Mater. 16 (8) (2017) 841–848.
[3] J. Liu, C. Xu, Z. Chen, et al., Progress in aqueous rechargeable batteries, Green Energy Environ. 3 (1) (2018) 20–41.
[4] M. Miao, J. Pan, T. He, et al., Molybdenum carbide-based electrocatalysts for hydrogen evolution reaction, Chem. Eur J. 23 (46) (2017) 10947–10961.
[5] X. Yu, B. Wang, D. Gong, et al., Graphene nanoribbons on highly porous 3D graphene for high-capacity and ultrastable Al-ion batteries, Adv. Mater. 29 (4) (2017) 1604118.
[6] B. Cao, S. Gao, Y. Ma, et al., Biomass-derived carbon-sulfur hybrids boosting electrochemical kinetics to achieve high potassium storage performance, J. Colloid Interface Sci. 661 (2024) 598–605.
[7] J. Li, Z. Liu, S. Han, et al., Hetero nucleus growth stabilizing zinc anode for high-biosecurity zinc-ion batteries, Nano-Micro Lett. 15 (1) (2023) 237.
[8] C. Xu, B. Li, H. Du, et al., Energetic zinc ion chemistry: the rechargeable zinc ion battery, Angew. Chem. Int. Ed. 51 (4) (2012) 933–935.
[9] J. Zheng, B. Zhang, X. Chen, et al., Critical solvation structures arrested active molecules for reversible Zn electrochemistry, Nano-Micro Lett. 16 (1) (2024) 145.
[10] Y. Chen, J. Li, Q. Zhu, et al., Two-dimensional organic supramolecule via hydrogen bonding and π–π stacking for ultrahigh capacity and long-life aqueous zinc–organic batteries, Angew. Chem. Int. Ed. 61 (37) (2022) e202116289.
[11] Z. Tie, L. Liu, S. Deng, et al., Proton insertion chemistry of a zinc–organic battery, Angew. Chem. Int. Ed. 59 (12) (2020) 4920–4924.
[12] Q. Li, L. Han, Q. Luo, et al., Towards understanding the corrosion behavior of zinc-metal anode in aqueous systems: from fundamentals to strategies, Batteries & Supercaps 5 (4) (2022) e202100417.
[13] P. Phummaree, M. Suttipong, T. Jaroonsteanpong, et al., Combined operando and ex-situ monitoring of the Zn/electrolyte interface in Zn-ion battery systems, Heliyon 9 (8) (2023) E18638.
[14] J. Ming, Z. Cao, W. Wahyudi, et al., New insights on graphite anode stability in rechargeable batteries: Li ion coordination structures prevail over solid electrolyte interphases, ACS Energy Lett. 3 (2) (2018) 335–340.
[15] H. Cheng, Z. Ma, P. Kumar, et al., High voltage electrolyte design mediated by advanced solvation chemistry toward high energy density and fast charging lithium-ion batteries, Adv. Energy Mater. (2304321) (2024) 1–15.
[16] L. Geng, J. Meng, X. Wang, et al., Eutectic electrolyte with unique solvation structure for high-performance zinc-ion batteries, Angew. Chem. Int. Ed. 61 (31) (2022) e202206717.
[17] T.C. Li, Y. Lim, X.L. Li, et al., A universal additive strategy to reshape electrolyte solvation structure toward reversible Zn storage, Adv. Energy Mater. 12 (15) (2022) 2103231.
[18] Z. Li, Y. Liao, Y. Wang, et al., A co-solvent in aqueous electrolyte towards ultralong-life rechargeable zinc-ion batteries, Energy Storage Mater. 56 (2023) 174–182.
[19] M. Qiu, P. Sun, K. Han, et al., Tailoring water structure with high-tetrahedral-entropy for antifreezing electrolytes and energy storage at −80 °C, Nat. Commun. 14 (1) (2023) 601.
[20] R. Wang, M. Yao, M. Yang, et al., Synergetic modulation on ionic association and solvation structure by electron-withdrawing effect for aqueous zinc-ion batteries, Proc. Natl. Acad. Sci. USA 120 (15) (2023) e2221980120.
[21] H. Liu, Z. Xin, B. Cao, et al., Polyhydroxylated organic molecular additives for durable aqueous zinc battery, Adv. Funct. Mater. 34 (4) (2024) 2309840.
[22] S. Chen, D. Ji, Q. Chen, et al., Coordination modulation of hydrated zinc ions to enhance redox reversibility of zinc batteries, Nat. Commun. 14 (1) (2023) 3526.
[23] H. Du, Y. Dong, Q.-J. Li, et al., A new zinc salt chemistry for aqueous zinc-metal batteries, Adv. Mater. 35 (25) (2023) 2210055.
[24] X. Xu, M. Song, M. Li, et al., A novel bifunctional zinc gluconate electrolyte for a stable Zn anode, Chem. Eng. J. 454 (2023) 140364.
[25] X. Li, Z. Chen, P. Ruan, et al., Inducing preferential growth of the Zn (002) plane by using a multifunctional chelator for achieving highly reversible Zn anodes, Nanoscale 16 (6) (2024) 2923–2930.
[26] C. Wang, Z. Pei, Q. Meng, et al., Toward flexible zinc-ion hybrid capacitors with superhigh energy density and ultralong cycling life: the pivotal role of ZnCl2 salt-based electrolytes, Angew. Chem. Int. Ed. 60 (2) (2021) 990–997.
[27] L. Suo, O. Borodin, T. Gao, et al., "Water-in-salt" electrolyte enables high-voltage aqueous lithium-ion chemistries, Science 350 (6263) (2015) 938–943.
[28] J. Zhang, M. Dolg, ABCluster: the artificial bee colony algorithm for cluster global optimization, Phys. Chem. Chem. Phys. 17 (37) (2015) 24173–24181.
[29] J. Zhang, M. Dolg, Global optimization of clusters of rigid molecules using the artificial bee colony algorithm, Phys. Chem. Chem. Phys. 18 (4) (2016) 3003–3010.
[30] X.L. Jiang, J.B. Wu, P.Y. Zhang, et al., First-principles investigation on multi-magnesium sulfide and magnesium sulfide clusters in magnesium-sulfide batteries, RSC Adv. 13 (30) (2023) 20926–20933.
[31] P.Y. Zhang, J.B. Wu, X.L. Jiang, et al., First-principles investigation on multi-sodium sulfide and sodium sulfide clusters in sodium-sulfide batteries, J. Electrochem. Soc. 170 (6) (2023) 060547.
[32] K. Raghavachari, Perspective on "Density functional thermochemistry. III. The role of exact exchange", Theor. Chem. Acc. 103 (3) (2000) 361–363.
[33] M.J. Frisch, G.W. Trucks, H.B. Schlegel, et al., Gaussian 16 Rev. B.01 [Z], 2016. Wallingford, CT.
[34] R. Ditchfield, W.J. Hehre, J.A. Pople, Self-consistent molecular-orbital methods. IX. An extended Gaussian-type basis for molecular-orbital studies of organic molecules, J. Chem. Phys. 54 (1971) 724–728.
[35] M.M. Francl, William J. Pietro, Warren J. Hehre, J. Binkley, Stephen Gordon, S. Mark, Douglas J. Defrees, John A. Pople, Self-consistent molecular orbital methods. XXIII. A polarization-type basis set for second-row elements, J. Chem. Phys. 77 (1982) 3654–3665.
[36] M.S. Gordon, J. Binkley, Stephen Pople, A. John, William J. Pietro, Warren J. Hehre, Self-consistent molecular-orbital methods. 22. Small split-valence basis sets for second-row elements, J. Am. Chem. Soc. 104 (1982) 2797–2803.
[37] P.C. Hariharan, J.A. Pople, The influence of polarization functions on molecular orbital hydrogenation energies, Theor. Chim. Acta 28 (1973) 213–222.
[38] W.J. Hehre, R. Ditchfield, J.A. Pople, Self-consistent molecular orbital methods. XII. Further extensions of Gaussian-type basis sets for use in molecular orbital studies of organic molecules, J. Chem. Phys. 56 (1972) 2257–2261.
[39] V.A. Rassolov, John A. Pople, Mark A. Ratner, Theresa L. Windus, 6-31G* basis set for atoms K through Zn, J. Chem. Phys. 109 (1998) 1223–1229.
[40] J.S. Murray, P. Politzer, The electrostatic potential: an overview, WIREs Computational Molecular Science 1 (2) (2011) 153–163.

[41] J.S. Murray, P. Politzer, Molecular electrostatic potentials and noncovalent interactions, WIREs Computational Molecular Science 7 (6) (2017) e1326.
[42] P. Politzer, J.S. Murray, The fundamental nature and role of the electrostatic potential in atoms and molecules, Theor. Chem. Acc. 108 (3) (2002) 134–142.
[43] Z. Liu, T. Lu, Q. Chen, Intermolecular interaction characteristics of the all-carboatomic ring, cyclo[18]carbon: focusing on molecular adsorption and stacking, Carbon 171 (2021) 514–523.
[44] T. Lu, F. Chen, Multiwfn: a multifunctional wavefunction analyzer, J. Comput. Chem. 33 (5) (2012) 580–592.
[45] T. Lu, F. Chen, Quantitative analysis of molecular surface based on improved Marching Tetrahedra algorithm, J. Mol. Graph. Model. 38 (2012) 314–323.
[46] J. Zhang, T. Lu, Efficient evaluation of electrostatic potential with computerized optimized code, Phys. Chem. Chem. Phys. 23 (36) (2021) 20323–20328.
[47] W. Humphrey, A. Dalke, K. Schulten, VMD: visual molecular dynamics, J. Mol. Graph. 14 (1) (1996) 33–38.
[48] M. Hartmann, T. Clark, R. Van Eldik, Hydration and water exchange of zinc(II) ions. Application of density functional theory, J. Am. Chem. Soc. 119 (33) (1997) 7843–7850.
[49] W. Rudolph W, C. Pye C, Zinc(II) hydration in aqueous solution. A Raman spectroscopic investigation and an ab-initio molecular orbital study, Phys. Chem. Chem. Phys. 1 (19) (1999) 4583–4593.